Supporting Information:

Anisotropic Contributions in the

Chromatographic Elution Behavior of Fullerenes

and Fullertubes

Emmanuel Bourret,[*,†,‡] Steven Stevenson,[¶,§] and Michel Côté[*,†,‡]

†*Département de Physique, Université de Montréal, Complexe des Sciences, 1375 Avenue Thérèse-Lavoie-Roux, Montréal, QC H2V 0B3, Canada*

‡*Institut Courtois, Université de Montréal, Complexe des Sciences, 1375 Avenue Thérèse-Lavoie-Roux, Montréal, QC H2V 0B3, Canada*

¶*Department of Chemistry and Biochemistry, Purdue University Fort Wayne, Fort Wayne, Indiana 46805, United States*

§*FIRST Molecules Research Center, Purdue University Fort Wayne, Fort Wayne, Indiana 46805, United States*

E-mail: emmanuel.bourret@umontreal.ca; michel.cote@umontreal.ca

Contents

1 Linear and Axially Symmetric Molecules Approximation

Consider a linear molecule that is aligned along the z-axis and possesses symmetric endcaps, i.e. $\alpha_{xx} = \alpha_{yy}$. The anisotropy of polarizability can be depicted through its parallel and perpendicular components. To demonstrate this, the anisotropy can be reformulated in the following manner:

$$
\begin{aligned}
(\Delta\alpha)^2 &= \frac{1}{2}\left[(\alpha_{xx} - \alpha_{yy})^2 + (\alpha_{xx} - \alpha_{zz})^2 + (\alpha_{yy} - \alpha_{zz})^2\right] \\
&= \frac{1}{2}\left[\alpha_{xx}^2 + \alpha_{yy}^2 - 2\alpha_{xx}\alpha_{yy} + \alpha_{xx}^2 + \alpha_{zz}^2 - 2\alpha_{xx}\alpha_{zz} + \alpha_{yy}^2 + \alpha_{zz}^2 - 2\alpha_{yy}\alpha_{zz}\right] \\
&= \alpha_{xx}^2 + \alpha_{yy}^2 + \alpha_{zz}^2 - \alpha_{xx}\alpha_{yy} - \alpha_{xx}\alpha_{zz} - \alpha_{yy}\alpha_{zz} \\
&= \alpha_{xx}^2 + \alpha_{yy}^2 + \alpha_{zz}^2 - \alpha_{xx}\alpha_{yy} - (\alpha_{xx} + \alpha_{yy})\alpha_{zz} \\
&= \alpha_{zz}^2 - (\alpha_{xx} + \alpha_{yy})\alpha_{zz} + \alpha_{xx}^2 + \alpha_{yy}^2 - \alpha_{xx}\alpha_{yy} \\
&= \alpha_{zz}^2 - (\alpha_{xx} + \alpha_{yy})\alpha_{zz} + \frac{1}{4}(\alpha_{xx}^2 + \alpha_{yy}^2 - \alpha_{xx}\alpha_{yy}) + \frac{3}{4}(\alpha_{xx}^2 + \alpha_{yy}^2 - \alpha_{xx}\alpha_{yy}) \\
&= \alpha_{zz}^2 - (\alpha_{xx} + \alpha_{yy})\alpha_{zz} + \frac{1}{4}(\alpha_{xx}^2 + \alpha_{yy}^2 - \alpha_{xx}\alpha_{yy} + 3\alpha_{xx}\alpha_{yy} - 3\alpha_{xx}\alpha_{yy}) \\
&\quad + \frac{3}{4}(\alpha_{xx}^2 + \alpha_{yy}^2 - \alpha_{xx}\alpha_{yy}) \\
&= \alpha_{zz}^2 - (\alpha_{xx} + \alpha_{yy})\alpha_{zz} + \frac{1}{4}(\alpha_{xx}^2 + \alpha_{yy}^2 + 2\alpha_{xx}\alpha_{yy}) + \frac{3}{4}(\alpha_{xx}^2 + \alpha_{yy}^2 - 2\alpha_{xx}\alpha_{yy}) \\
&= \alpha_{zz}^2 - (\alpha_{xx} + \alpha_{yy})\alpha_{zz} + \frac{1}{4}(\alpha_{xx} + \alpha_{yy})^2 + \frac{3}{4}(\alpha_{xx}^2 - \alpha_{yy}^2)^2 \\
&= \left[\alpha_{zz} - \frac{\alpha_{xx} + \alpha_{yy}}{2}\right]^2 + \frac{3}{4}(\alpha_{xx} - \alpha_{yy})^2
\end{aligned}
$$

The expressions for the anisotropic polarizability can then be given as $\Delta\alpha = \alpha_{\parallel} - \alpha_{\perp}$. Even when the molecule is not linear and the endcaps lack symmetry, i.e. $\alpha_{xx} \neq \alpha_{yy}$, the system can occasionally be handled as though the molecule were, provided the difference between α_{xx} and α_{yy} is minimal. This is typically applicable to fullerenes, given their enclosed cage structure and the fact that the curvature is only induced by the 12 pentagons, which restrict the variations between the components.

The polarizabilities discussed so far result from a static electric field. Alternatively, when the applied electric field oscillates in time, it becomes necessary to consider the frequency-dependent polarizability $\alpha(iu)$, where u is a real number. The utilization of the imaginary frequency iu, whose physical interpretation is a matter of debate, offers the advantage of making the mathematical entity $\alpha(iu)$ well defined. This allows the polarizabilities to be much more well-behaved than those at real frequencies, decreasing monotonically from the static polarizability as $u = 0$ to zeros as $u \to \infty$.[S1] For a molecule A, a common approximation involving the static polarizability $\alpha^A(0)$ and the ionization energy U_A is as follows:[S2]

$$\alpha^A(iu) \approx \alpha^A(0)\frac{U_A^2}{U_A^2 + u^2} \tag{1}$$

Given that the formulations for the isotropic and anisotropic dispersion coefficients, as initially developed by Stone and Tough[S3], were articulated using dynamic polarizabilities, conversion to static polarizabilities becomes imperative. This necessity arises because, within the temporal framework of molecular dynamics, electron movements appear instantaneous. Consequently, to recast these dynamic polarizabilities into static terms, we need to employ eq 1 and then apply the Casimir-Polder type integral:[S4]

$$\frac{1}{a + b} = \frac{2}{\pi}\int_0^\infty \frac{ab}{(a^2 + \nu^2)(b^2 + \nu^2)}d\nu \tag{2}$$

which is valid for positive a and b. Consequently, the isotropic and anisotropic dispersion coefficients can be delineated as follows

$$
\begin{aligned}
C_6 &= \frac{3\hbar}{\pi}\int_0^\infty \overline{\alpha}^A(i\nu)\overline{\alpha}^B(i\nu)d\nu & &\approx \frac{3}{2}\frac{U_AU_B}{U_A + U_B}\overline{\alpha}^A\overline{\alpha}^B \\
\gamma_{202}C_6 &= \frac{\hbar}{\pi}\int_0^\infty \Delta\alpha^A(i\nu)\overline{\alpha}^B(i\nu)d\nu & &\approx \frac{1}{2}\frac{U_AU_B}{U_A + U_B}\Delta\alpha^A\overline{\alpha}^B \\
\gamma_{022}C_6 &= \frac{\hbar}{\pi}\int_0^\infty \overline{\alpha}^A(i\nu)\Delta\alpha^B(i\nu)d\nu & &\approx \frac{1}{2}\frac{U_AU_B}{U_A + U_B}\overline{\alpha}^A\Delta\alpha^B \\
\gamma_{22}C_6 &= \frac{\hbar}{\pi}\int_0^\infty \Delta\alpha^A(i\nu)\Delta\alpha^B(i\nu)d\nu & &\approx \frac{1}{2}\frac{U_AU_B}{U_A + U_B}\Delta\alpha^A\Delta\alpha^B
\end{aligned}
\tag{3}
$$

2   Statistical Measures

Consider x_i, an estimate of the value $\hat{x}_i$.

- Error: $e_i = x_i - \hat{x}_i$

- Mean error (ME): $\text{ME} = \dfrac{1}{n} \sum_i e_i$

- Mean absolute error (MAE): $\text{MAE} = \dfrac{1}{n} \sum_i |e_i|$

- Standard deviation (SD): $\text{SD} = \sqrt{\dfrac{1}{n} \sum_i (e_i - \text{ME})^2}$

- Maximum absolute error (AMAX): $\text{AMAX} = \max\{|e_i|\}$

3   Convergence Studies

To ascertain the level of theory needed to calculate the properties of interest, a convergence study was conducted (refer to Table S1), during which we evaluated the orbital energy values following the structural relaxation of the C_{60} molecule in vacuum conditions. Using the def2-QZVP basis set as a benchmark, we achieved convergence of the orbital energies to within $0.1\,eV$ using def2-SVP, confirming the adequacy of this basis set.

Table S1: Basis set convergence of HOMO and LUMO Energies, Energy Gap, and Ionization Energy of fullerene C_{60} with B3LYP functional.

Basis set	E_{HOMO} [eV]	E_{LUMO} [eV]	ΔE_{HL} [eV]	IE [eV]
def2-SVP	-6.325	-3.592	2.732	7.527
def2-TZVP	-6.378	-3.653	2.725	7.548
def2-QZVP	-6.384	-3.658	2.726	7.548

As with orbital energies, the use of the def2-SVP basis set ensures that the vertical ionization energy values (as calculated per the main text) achieve a convergence with an unsigned error of less than $0.1\,eV$ (refer to Table S1).

Table S2: Isotropic polarizability $\overline{\alpha}$ of fullerene C_{60} evaluated at different levels of theory.

Method	Basis set (structure)	Basis set ($\overline{\alpha}$)	$\overline{\alpha}$ [Å^3]
B3LYP	def2-SVP	def2-SVP	73.95
B3LYP	def2-TZVP	def2-TZVP	79.61
B3LYP	def2-QZVP	def2-QZVP	80.67
B3LYP	def2-SVP	def2-SVPD	81.56
B3LYP	def2-SVP	def2-TZVPPD	82.25
B3LYP	def2-SVP	def2-QZVPPD	82.28
B3LYP	def2-QZVP	def2-QZVPPD	81.10
Expt.			$76.5 \pm 8,$[a] 79 ± 4[b]

[a]Molecular beam deflection (Ref. S5).

[b]Mass spectrometry (Ref. S6).

For calculating polarizabilities, the optimal computational efficiency was achieved through

a multilevel approach where the structures were optimized using the def2-SVP basis set and the polarizabilities were determined by incorporating diffuse functions via the def2-SVPD basis set. This particular set was selected due to its rapid and monotonous convergence in the isotropic polarizability calculations for fullerenes. In comparison to def2-QZVPPD, the def2-SVPD basis set maintains an error below 1 (refer to Table S2).

4 DFT Calculated Values for the Fullerenes and Fuller-tubes Investigated

Table S3: Overview and comparison of the I_h fullerenes and the three series of fullertubes with C_{60} endcaps up to 320 atoms. All values are calculated using DFT (see the Computational Details section for details).

Fullerene	ρ_B [Å]	E_{HOMO} [eV]	E_{LUMO} [eV]	ΔE_{HL} [eV]	IE [eV]	α_{xx} [Å^3]	α_{yy} [Å^3]	α_{zz} [Å^3]	μ [D]
				I_h *fullerenes*					
C_{20}-I_h	2.01	−5.389	−3.479	1.910	7.149	26.63	27.62	28.18	0.00
C_{60}-I_h	3.55	−6.325	−3.592	2.732	7.527	81.56	81.56	81.56	0.00
C_{80}-I_h	4.04	−5.612	−4.843	0.768	6.687	129.64	130.48	131.64	0.00
C_{180}-I_h	6.04	−6.058	−3.748	2.310	6.834	300.49	300.49	300.49	0.00
C_{240}-I_h	6.96	−5.742	−3.726	2.016	6.428	430.13	430.13	430.13	0.00
C_{320}-I_h	7.93	−4.881	−4.515	0.367	5.485	733.61	737.85	740.80	0.00
				C_{60+10n} *fullertubes*					
C_{70}-D_{5h}	3.57	−6.260	−3.595	2.665	7.389	97.54	97.54	107.67	0.00
C_{80}-D_{5d}	3.55	−5.272	−4.309	0.963	6.350	105.57	105.57	136.16	0.00
C_{90}-D_{5h}	3.50	−5.635	−3.703	1.933	6.664	116.30	116.30	166.79	0.00
C_{100}-D_{5d}	3.47	−5.776	−3.602	2.175	6.758	130.69	130.70	204.95	0.00
C_{110}-D_{5h}	3.44	−5.128	−4.092	1.036	6.069	144.90	144.91	247.11	0.00
C_{120}-D_{5d}	3.46	−5.289	−3.851	1.438	6.195	150.49	150.50	288.68	0.00
C_{130}-D_{5h}	3.44	−5.493	−3.674	1.819	6.366	163.81	163.83	340.98	0.00
C_{140}-D_{5d}	3.44	−5.022	−4.043	0.979	5.865	177.47	177.48	398.14	0.00
C_{150}-D_{5h}	3.44	−5.080	−3.940	1.141	5.896	184.10	184.11	453.05	0.00
C_{160}-D_{5d}	3.44	−5.287	−3.721	1.566	6.077	196.59	196.61	521.05	0.00
C_{170}-D_{5h}	3.43	−4.954	−4.017	0.938	5.722	209.96	209.98	595.35	0.00
C_{180}-D_{5d}	3.44	−4.940	−4.004	0.936	5.685	217.32	217.33	664.73	0.00
C_{190}-D_{5h}	3.44	−5.123	−3.771	1.353	5.848	229.38	229.39	750.47	0.00
C_{200}-D_{5d}	3.43	−4.905	−4.002	0.903	5.611	242.32	242.34	842.71	0.00
C_{210}-D_{5h}	3.44	−4.837	−4.051	0.786	5.525	250.33	250.35	928.30	0.00
C_{220}-D_{5d}	3.44	−5.002	−3.845	1.157	5.672	262.10	262.13	1033.01	0.00

Fullerene	ρ_B [Å]	E_{HOMO} [eV]	E_{LUMO} [eV]	ΔE_{HL} [eV]	IE [eV]	α_{xx} [Å^3]	α_{yy} [Å^3]	α_{zz} [Å^3]	μ [D]
C$_{230}$-D_{5h}	3.44	−4.867	−3.992	0.875	5.523	274.78	274.81	1144.67	0.00
C$_{240}$-D_{5d}	3.44	−4.759	−4.088	0.671	5.399	283.11	283.13	1247.39	0.00
C$_{250}$-D_{5h}	3.44	−4.908	−3.904	1.004	5.533	294.78	294.81	1372.61	0.00
C$_{260}$-D_{5d}	3.44	−4.836	−3.985	0.851	5.449	307.24	307.27	1504.53	0.00
C$_{270}$-D_{5h}	3.44	−4.641	−4.147	0.494	5.241	320.13	320.16	1642.88	0.00
C$_{280}$-D_{5d}	3.44	−4.833	−3.950	0.883	5.419	327.44	327.47	1772.71	0.00
C$_{290}$-D_{5h}	3.44	−4.811	−3.981	0.831	5.388	339.87	339.90	1926.52	0.00
C$_{300}$-D_{5d}	3.44	−4.636	−4.126	0.510	5.201	352.43	352.48	2085.89	0.00
C$_{310}$-D_{5h}	3.44	−4.771	−3.988	0.783	5.324	360.07	360.10	2236.68	0.00
C$_{320}$-D_{5d}	3.44	−4.790	−3.977	0.813	5.334	372.19	372.23	2412.32	0.00
C$_{60+12n}$ *fullertubes*									
C$_{72}$-D_{6d}	3.24	−6.149	−3.678	2.472	7.272	86.41	109.62	109.62	0.00
C$_{84}$-D_2	3.19	−5.935	−3.587	2.348	6.989	100.52	124.67	142.18	0.00
C$_{96}$-D_2	3.70	−5.789	−3.653	2.136	6.788	123.33	129.23	179.64	0.00
C$_{108}$-D_2	3.20	−5.627	−3.646	1.981	6.577	124.80	155.97	225.44	0.00
C$_{120}$-D_2	3.67	−5.518	−3.693	1.825	6.425	143.61	165.55	274.03	0.00
C$_{132}$-D_2	3.66	−5.398	−3.768	1.631	6.267	161.92	174.72	329.50	0.00
C$_{144}$-D_2	3.35	−5.316	−3.769	1.547	6.150	166.03	197.85	392.42	0.00
C$_{156}$-D_2	3.67	−5.245	−3.801	1.444	6.048	188.33	203.30	460.19	0.00
C$_{168}$-D_2	3.63	−5.171	−3.844	1.327	5.946	200.44	218.24	536.48	0.00
C$_{180}$-D_2	3.52	−5.119	−3.852	1.267	5.868	208.29	237.47	619.01	0.00
C$_{192}$-D_2	3.64	−5.067	−3.876	1.190	5.791	232.34	240.60	709.38	0.00
C$_{204}$-D_2	3.64	−5.020	−3.903	1.118	5.723	239.28	260.64	807.82	0.00
C$_{216}$-D_2	3.60	−4.981	−3.912	1.070	5.664	250.33	276.53	913.30	0.00
C$_{228}$-D_2	3.64	−4.944	−3.930	1.014	5.607	275.84	277.67	1027.63	0.00
C$_{240}$-D_2	3.64	−4.912	−3.947	0.965	5.558	277.97	302.42	1150.02	0.00
C$_{252}$-D_2	3.59	−4.881	−3.956	0.925	5.510	292.29	315.23	1281.52	0.00
C$_{264}$-D_2	3.64	−4.854	−3.970	0.884	5.467	315.03	319.27	1421.75	0.00
C$_{276}$-D_2	3.59	−4.828	−3.982	0.847	5.427	317.26	343.88	1570.63	0.00
C$_{288}$-D_2	3.64	−4.805	−3.991	0.814	5.389	334.36	353.14	1729.05	0.00

Table S3 (continued)

Fullerene	ρ_B [Å]	E_{HOMO} [eV]	E_{LUMO} [eV]	ΔE_{HL} [eV]	IE [eV]	α_{xx} [Å^3]	α_{yy} [Å^3]	α_{zz} [Å^3]	μ [D]
C$_{300}$-D_2	3.64	-4.784	-4.001	0.783	5.355	352.21	362.44	1897.16	0.00
C$_{312}$-D_2	3.60	-4.764	-4.010	0.753	5.322	356.79	384.58	2074.60	0.00
C$_{60+18n}$ *fullertubes*									
C$_{78}$-D_{3h}	3.53	-5.993	-3.554	2.440	7.077	104.11	104.12	126.52	0.00
C$_{96}$-D_{3d}	3.54	-5.741	-3.671	2.069	6.736	124.96	124.98	183.80	0.00
C$_{114}$-D_{3h}	3.53	-5.543	-3.662	1.881	6.466	145.70	145.74	254.45	0.00
C$_{132}$-D_{3d}	3.56	-5.386	-3.754	1.632	6.250	166.24	166.28	3378.78	0.00
C$_{150}$-D_{3h}	3.57	-5.269	-3.759	1.510	6.082	186.20	186.24	437.48	0.00
C$_{168}$-D_{3d}	3.57	-5.174	-3.809	1.365	5.943	206.75	206.80	553.37	0.00
C$_{186}$-D_{3h}	3.57	-5.095	-3.819	1.276	5.826	226.84	226.89	685.57	0.00
C$_{204}$-D_{3d}	3.57	-5.030	-3.849	1.181	5.726	246.87	246.93	835.62	0.00
C$_{222}$-D_{3h}	3.57	-4.974	-3.860	1.114	5.641	266.85	266.90	1004.49	0.00
C$_{240}$-D_{3d}	3.57	-4.926	-3.879	1.047	5.565	286.65	286.72	1192.46	0.00
C$_{258}$-D_{3h}	3.58	-4.884	-3.889	0.995	5.498	306.69	306.75	1401.50	0.00
C$_{276}$-D_{3d}	3.58	-4.847	-3.902	0.945	5.438	326.58	326.64	1631.51	0.00
C$_{294}$-D_{3h}	3.58	-4.814	-3.911	0.904	5.385	346.28	346.35	1883.02	0.00
C$_{312}$-D_{3d}	3.58	-4.785	-3.920	0.865	5.336	366.28	366.34	2157.99	0.00

5 DFT Calculated Values for the Fullerenes and Fuller-tubes Experimentally Isolated

Table S4: Overview and comparison of the fullerenes and fullertubes experimentaly isolated in this study. All values are calculated using DFT (see the Computational Details section for details).

| Eluite	E_{HOMO} [eV]	E_{LUMO} [eV]	ΔE_{HL} [eV]	IE [eV]	α_{xx} [Å^3]	α_{yy} [Å^3]	α_{zz} [Å^3]	μ [D]
C_{60}-I_h	-6.325	-3.592	2.732	7.527	81.56	81.56	81.56	0.00
C_{70}-D_{5h}	-6.260	-3.595	2.665	7.389	97.54	97.54	107.67	0.00
C_{76}-D_2	-5.773	-3.820	1.953	6.872	98.98	111.98	119.83	0.00
C_{78}-$C_{2v}(2)$	-5.955	-3.957	1.998	7.038	104.48	110.13	123.89	0.15
C_{84}-$D_2(22)$	-5.969	-4.015	1.954	7.025	117.66	124.02	128.70	0.00
C_{90}-$C_1(32)$	-5.912	-4.109	1.803	6.936	119.85	140.42	142.20	0.31
C_{90}-D_{5h}	-5.635	-3.703	1.933	6.664	116.30	116.30	166.79	0.00
C_{96}-D_{3d}	-5.741	-3.671	2.069	6.736	124.96	124.98	183.80	0.00
C_{100}-D_{5d}	-5.776	-3.602	2.175	6.758	130.69	130.70	204.95	0.00
C_{114}-D_{3h}	-5.543	-3.662	1.881	6.466	145.70	145.74	254.45	0.00
C_{120}-D_{5d}	-5.289	-3.851	1.438	6.195	150.49	150.50	288.68	0.00
C_{130}-D_{5h}	-5.493	-3.674	1.819	6.366	163.81	163.83	340.98	0.00

6   Polarizabilities
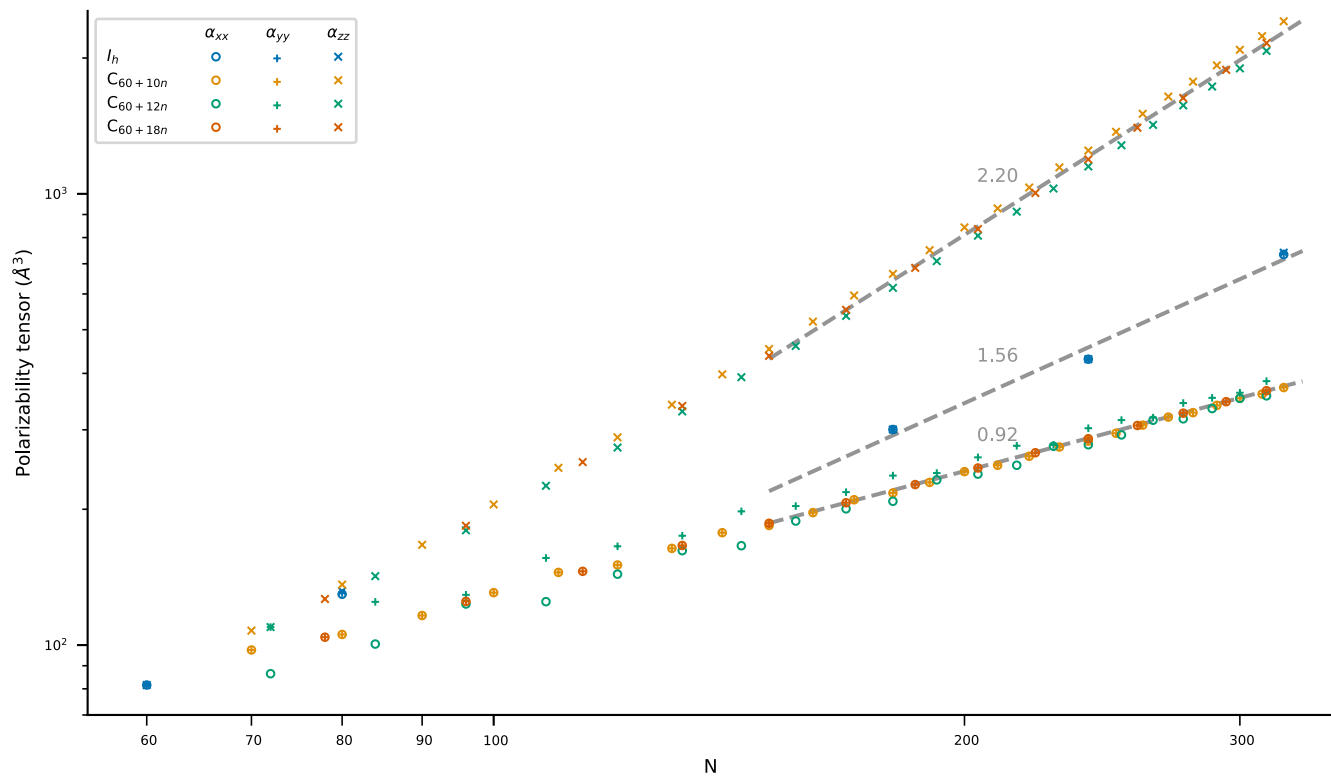
Figure S1: Log-log plot of the calculated polarizability tensor components for I_h fullerenes (blue) and three series of fullertubes with C_{60} endcaps (orange, green, red) vs N the number of carbon atoms. The slopes for $N \geq 150$ are presented in gray.

7   PAHs as Functional Group

Table S5: Overview and comparison of the PAHs that can potentially be used as functional groups . All values are calculated using DFT (see the Computational Details section for details).

Rings	Functional Group	IE [eV]	α_{xx} [Å^3]	α_{yy} [Å^3]	α_{zz} [Å^3]	μ [D]	$\overline{\alpha}$ [Å^3]	$\Delta\alpha$ [Å^3]	$|A_{\mathrm{ani}}/A_{\mathrm{iso}}|$ [10^{-2}]
2	Naphthalene	7.917	9.40	18.33	25.19	0.00	17.64	13.72	4.26
3	Phenanthrene	7.647	12.33	26.15	38.15	0.01	25.54	22.38	2.42
3	Anthracene	7.106	12.41	24.77	43.48	0.00	26.88	27.09	0.15
4	Pyrene	7.161	13.40	31.45	43.66	0.00	29.50	26.37	2.08
4	Triphenylene	7.612	15.16	41.87	41.87	0.00	32.66	26.71	3.65
4	Benzo[c]phen-anthrene	7.299	16.07	37.14	47.81	0.09	33.67	27.98	3.27
4	Chrysene	7.260	15.25	32.34	55.77	0.00	34.45	35.23	0.45
4	Benz[a]anthracene	7.060	15.31	33.15	58.03	0.03	35.50	37.16	0.95
4	Tetracene	6.562	15.40	31.43	66.69	0.00	37.84	45.45	4.19
5	Benzo[e]pyrene	7.126	16.22	47.03	47.69	0.05	36.98	31.15	3.06
5	Perylene	6.652	16.20	43.34	55.28	0.00	38.27	34.68	1.84
5	Benzo[a]pyrene	6.793	16.31	37.74	64.65	0.01	39.57	41.95	1.22
5	Picene	7.126	18.16	39.24	74.27	0.02	43.89	49.09	2.43
5	Dibenzo[a,j]-anthracene	7.041	18.18	44.25	69.85	0.03	44.09	44.75	0.30
5	Dibenzo[a,h]-anthracene	7.003	18.20	39.90	76.44	0.00	44.85	50.98	2.81
5	Pentacene	6.173	18.39	38.35	94.52	0.00	50.42	68.37	7.67
6	Benzo[ghi]perylene	6.869	17.27	50.82	55.57	0.04	41.22	36.16	2.40
6	Anthanthrene	6.535	17.37	43.40	72.38	0.00	44.38	47.66	1.50
6	Zethrene	6.130	19.17	49.18	94.71	0.00	54.35	65.87	4.43
6	Hexacene	5.882	21.37	45.53	126.52	0.00	64.47	95.39	10.61
7	Coronene	7.086	18.34	58.50	58.50	0.00	45.11	40.16	2.15
7	Trinaphthylene	6.870	23.95	84.51	84.52	0.00	64.33	60.57	1.16
10	Ovalene	6.419	23.24	75.99	94.07	0.00	64.43	63.75	0.21

Table S5 (continued)

Rings	Functional Group	IE [eV]	α_{xx} [Å^3]	α_{yy} [Å^3]	α_{zz} [Å^3]	μ [D]	$\overline{\alpha}$ [Å^3]	$\Delta\alpha$ [Å^3]	$|A_{\mathrm{ani}}/A_{\mathrm{iso}}|$ [10^{-2}]
13	Hexabenzo-[bc,ef,hi,kl,no,qr]-coronene	6.600	29.55	111.31	111.32	0.00	84.06	81.77	0.54

Table S6: Theoritical prediction of retention times for two isomers of C_{90} on stationary phases with different PAHs as functional groups.

Functional Group	Predicted t_R		Δt_R
	C_{90}-D_{5h}	C_{90}-$C_1(32)$	
	[min]	[min]	[min]
Naphthalene	6.04	6.10	-0.06
Anthracene	9.30	8.88	0.42
Pyrene	11.71	10.86	0.85
Triphenylene	17.53	15.01	2.52
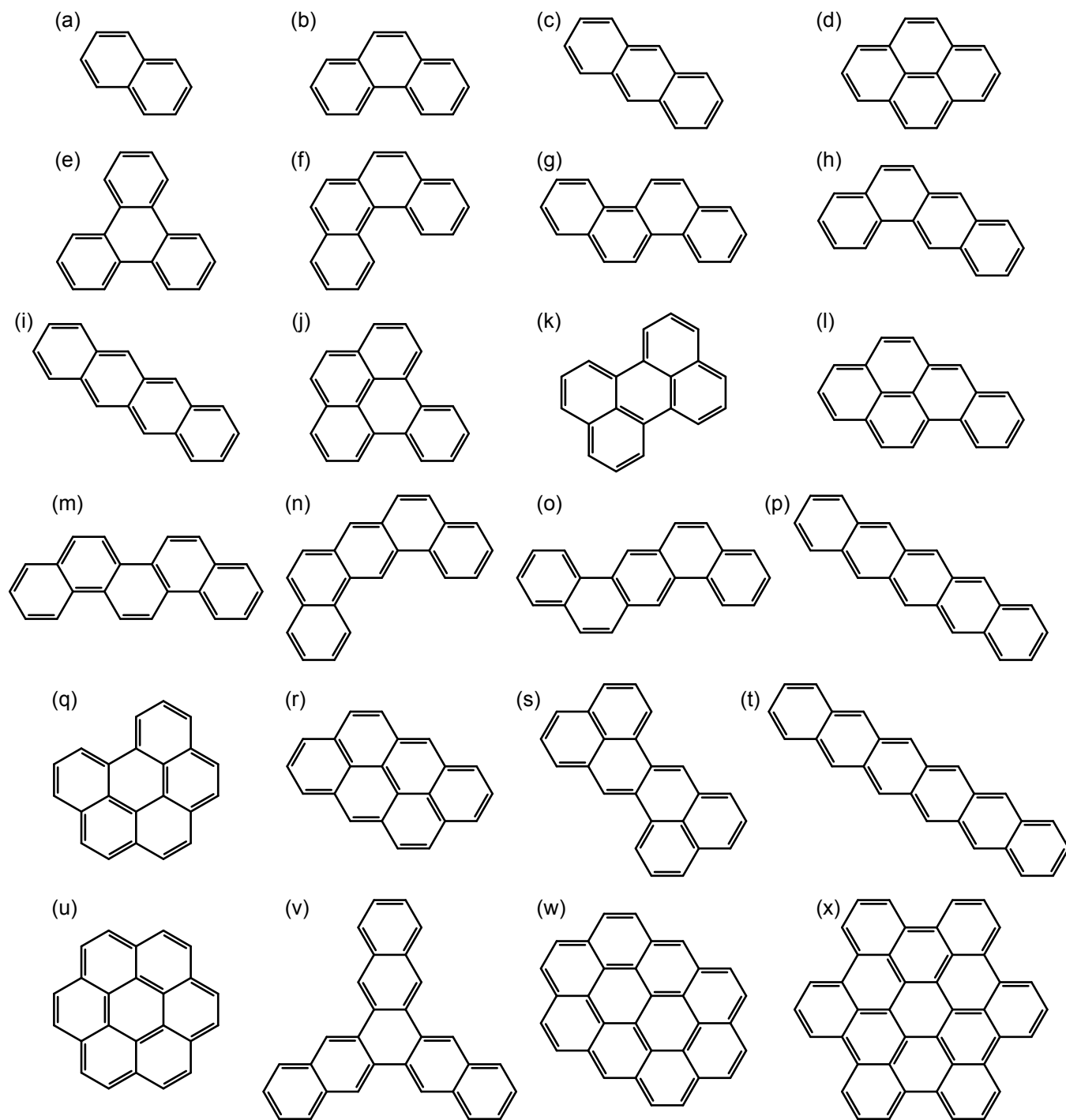
Figure S2: Structures of PAHs presented in Table S5: (a) Naphthalene, (b) Phenanthrene, (c) Anthracene, (d) Pyrene, (e) Triphenylene, (f) Benzo[c]phenanthrene, (g) Chrysene, (h) Benz[a]anthracene, (i) Tetracene, (j) Benzo[e]pyrene, (k) Perylene, (l) Benzo[a]pyrene, (m) Picene, (n) Dibenzo[a,j]anthracene, (o) Dibenzo[a,h]anthracene, (p) Pentacene, (q) Benzo[ghi]perylene, (r) Anthanthrene, (s) Zethrene, (t) Hexacene, (u) Coronene, (v) Trinaphthylene, (w) Ovalene, (x) Hexabenzo[bc,ef,hi,kl,no,qr]coronene.
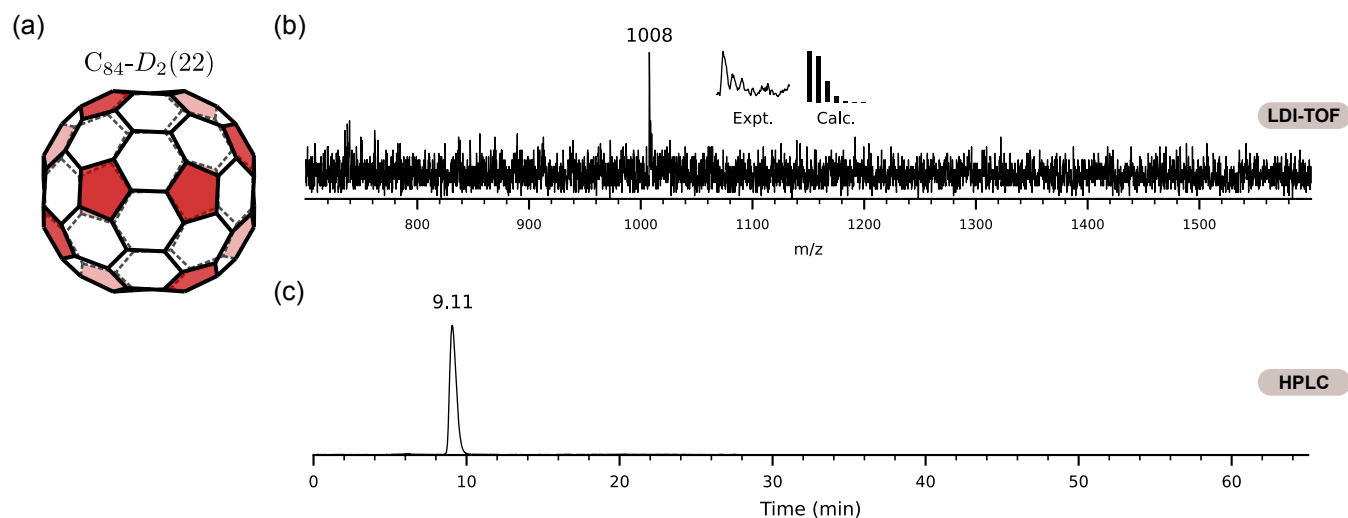
8 Structure Identification
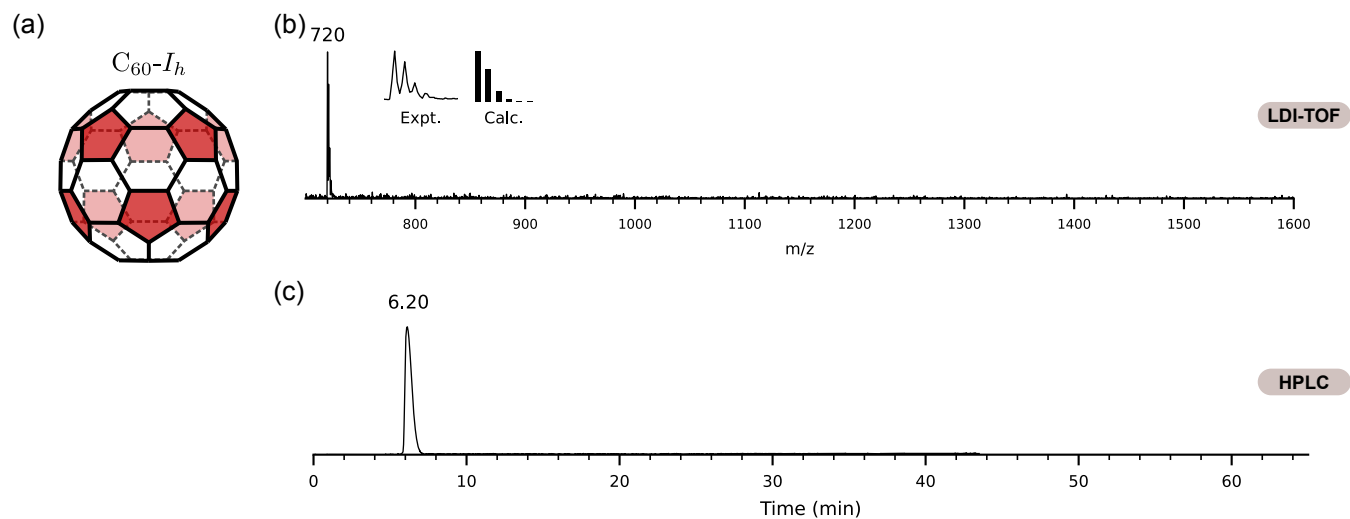
Figure S3: Characterization of purified C_{60}-I_h fullerene via (a) DFT optimized structure, (b) LDI-TOF mass spectrometry, and (c) chromatogram with online HPLC-PDA spectra. HPLC conditions: column, PYE (10 mm I.D.$\times$250 mm); mobile phase, o-xylene; temperature, 22 °C; flow-rate, 3.06 mL/min; detection, UV at 500 nm; amount injected, 1000 µL.
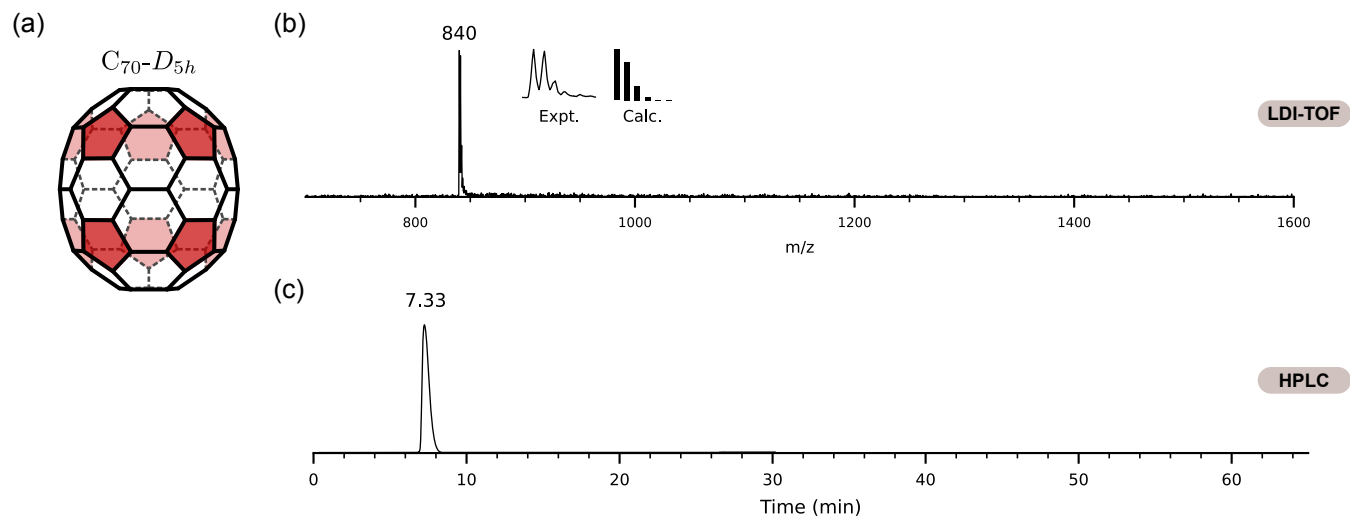
Figure S4: Characterization of purified C_{70}-D_{5h} fullerene via (a) DFT optimized structure, (b) LDI-TOF mass spectrometry, and (c) chromatogram with online HPLC-PDA spectra. HPLC conditions as in Figure S3.
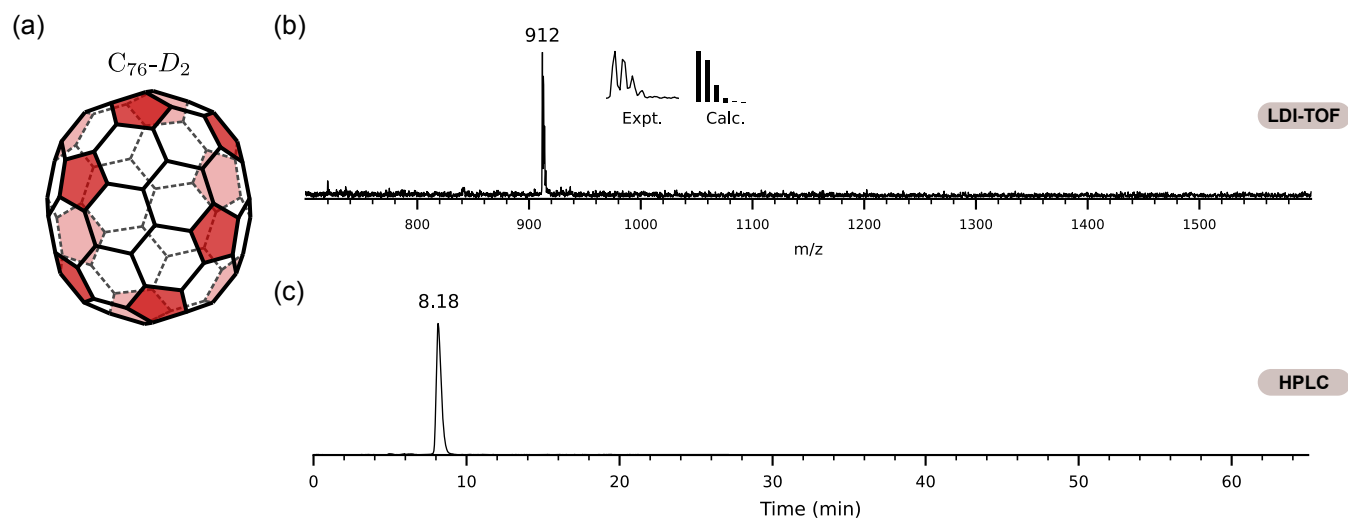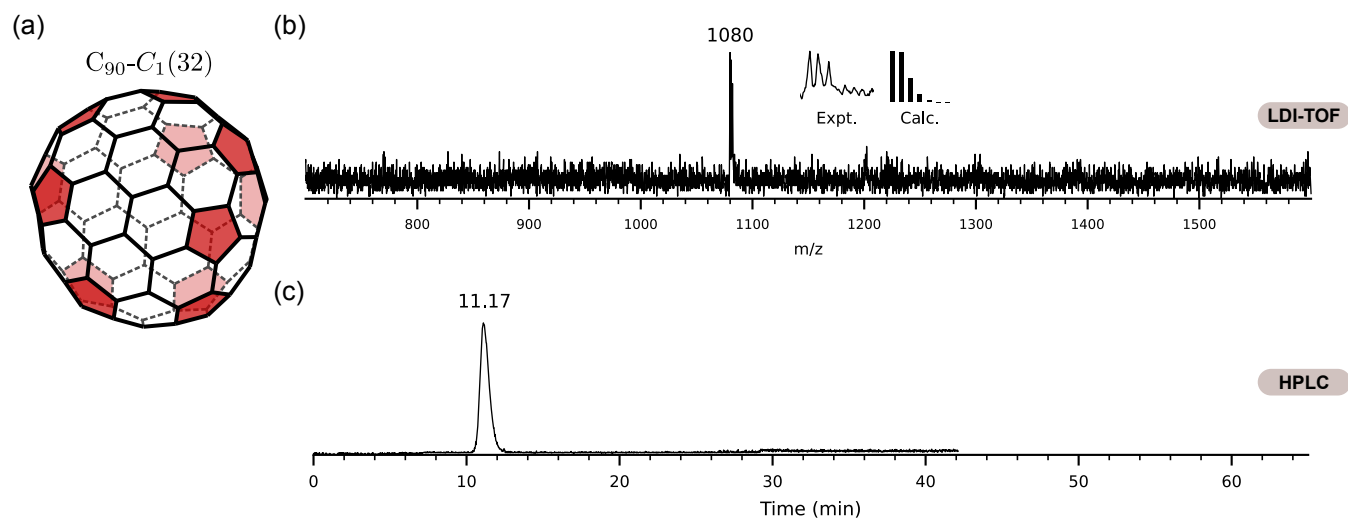
Figure S5: Characterization of purified C_{76}-D_2 fullerene via (a) DFT optimized structure, (b) LDI-TOF mass spectrometry, and (c) chromatogram with online HPLC-PDA spectra. HPLC conditions as in Figure S3.
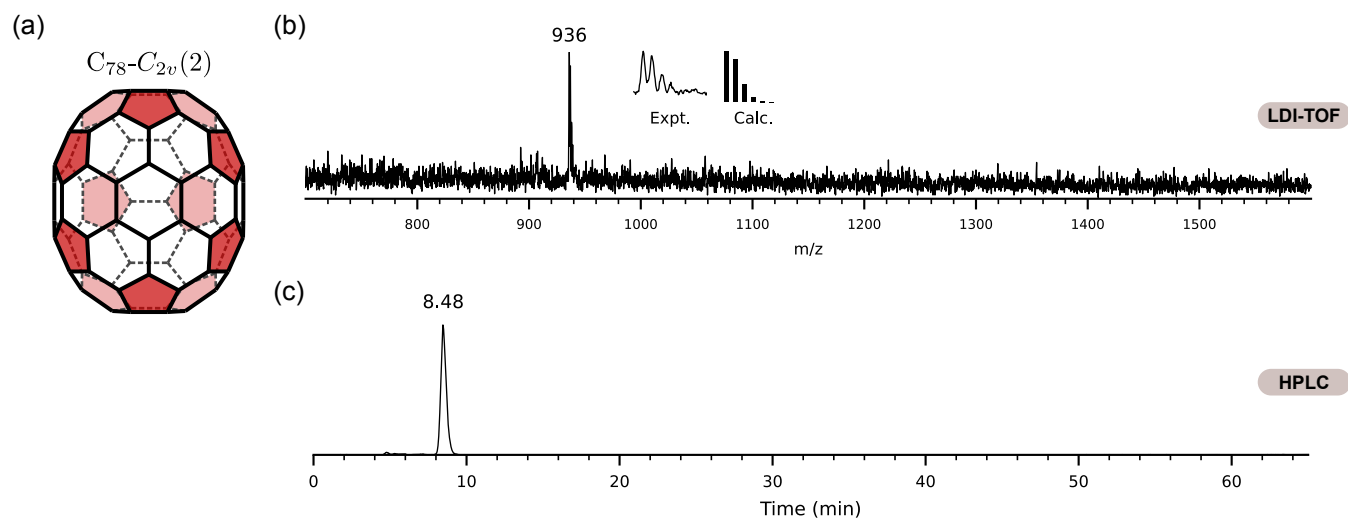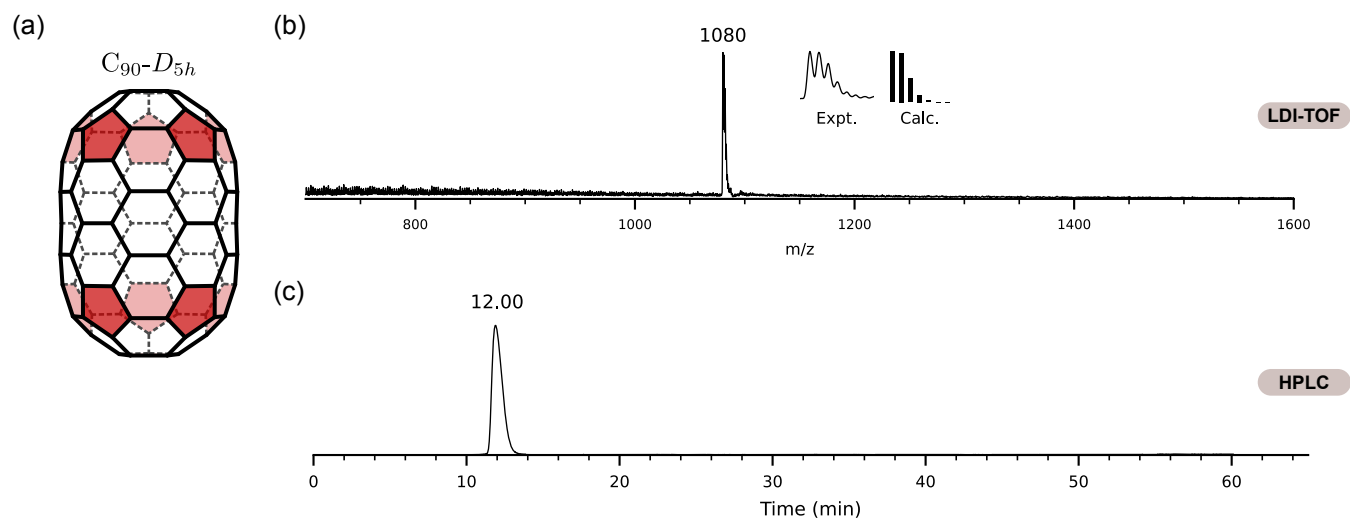

Figure S6: Characterization of purified C_{78}-$C_{2v}(2)$ fullerene via (a) DFT optimized structure, (b) LDI-TOF mass spectrometry, and (c) chromatogram with online HPLC-PDA spectra. HPLC conditions as in Figure S3.

Figure S7: Characterization of purified C$_{84}$-D_2(22) fullerene via (a) DFT optimized structure, (b) LDI-TOF mass spectrometry, and (c) chromatogram with online HPLC-PDA spectra. HPLC conditions as in Figure S3.
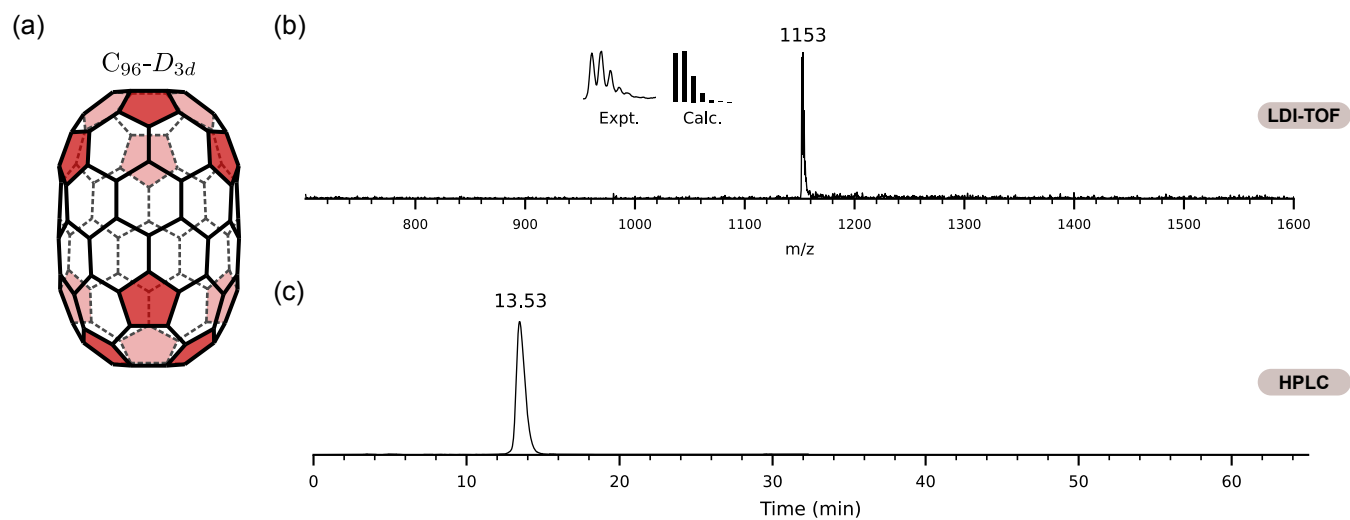

Figure S8: Characterization of purified C$_{90}$-C_1(32) fullerene via (a) DFT optimized structure, (b) LDI-TOF mass spectrometry, and (c) chromatogram with online HPLC-PDA spectra. HPLC conditions as in Figure S3.

Figure S9: Characterization of purified C$_{90}$-D_{5h} fullerene via (a) DFT optimized structure, (b) LDI-TOF mass spectrometry, and (c) chromatogram with online HPLC-PDA spectra. HPLC conditions as in Figure S3.
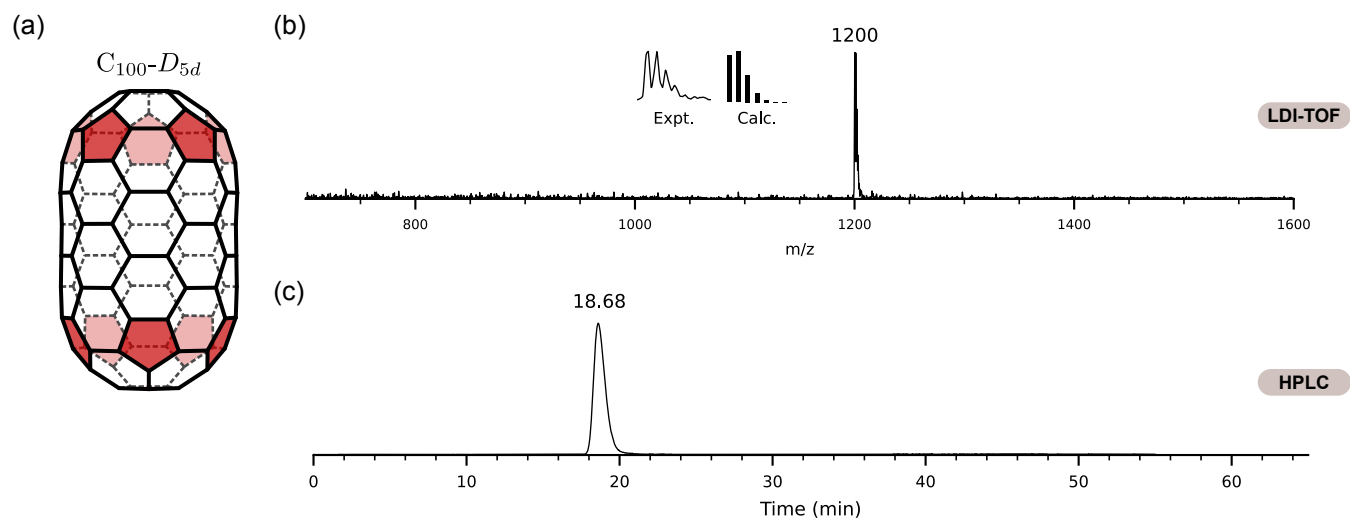

Figure S10: Characterization of purified C$_{96}$-D_{3d} fullerene via (a) DFT optimized structure, (b) LDI-TOF mass spectrometry, and (c) chromatogram with online HPLC-PDA spectra. HPLC conditions as in Figure S3.

Figure S11: Characterization of purified C_{100}-D_{5d} fullerene via (a) DFT optimized structure, (b) LDI-TOF mass spectrometry, and (c) chromatogram with online HPLC-PDA spectra. HPLC conditions as in Figure S3.
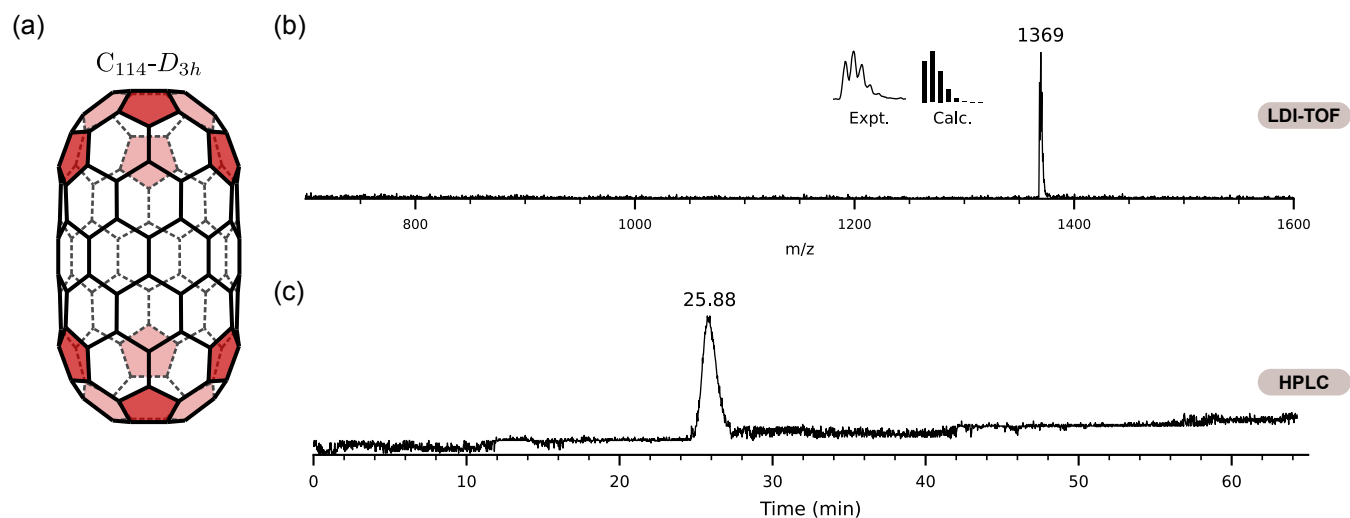

Figure S12: Characterization of purified C_{114}-D_{3h} fullerene via (a) DFT optimized structure, (b) LDI-TOF mass spectrometry, and (c) chromatogram with online HPLC-PDA spectra. HPLC conditions as in Figure S3.
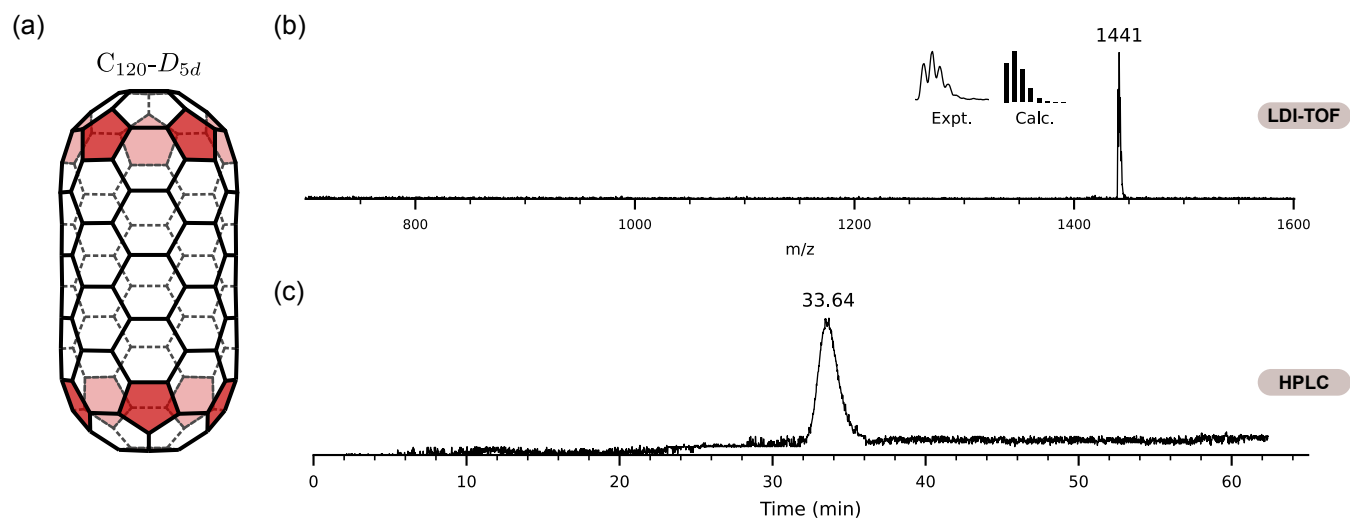
(a)

$C_{120}\text{-}D_{5d}$

(b)

1441

Expt.   Calc.

LDI-TOF

800   1000   1200   1400   1600

m/z

(c)

33.64

HPLC

0   10   20   30   40   50   60

Time (min)

Figure S13: Characterization of purified $C_{120}\text{-}D_{5d}$ fullerene via (a) DFT optimized structure, (b) LDI-TOF mass spectrometry, and (c) chromatogram with online HPLC-PDA spectra. HPLC conditions as in Figure S3.
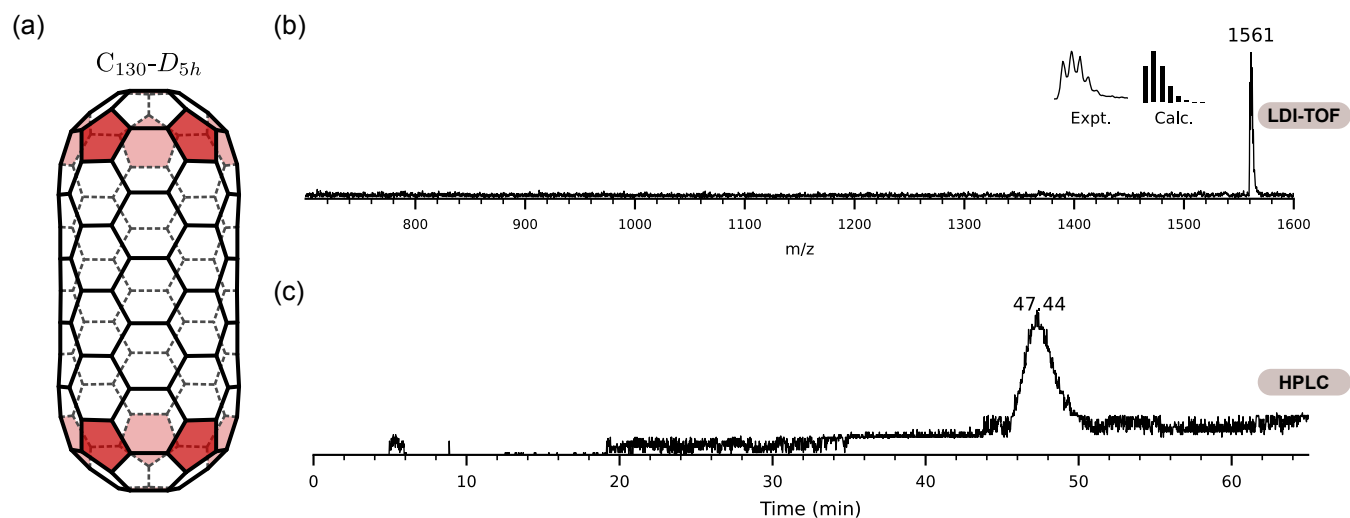
(a)

$C_{130}\text{-}D_{5h}$

(b)

1561

Expt.   Calc.

LDI-TOF

800   900   1000   1100   1200   1300   1400   1500   1600

m/z

(c)

47.44

HPLC

0   10   20   30   40   50   60

Time (min)

Figure S14: Characterization of purified $C_{130}\text{-}D_{5h}$ fullerene via (a) DFT optimized structure, (b) LDI-TOF mass spectrometry, and (c) chromatogram with online HPLC-PDA spectra. HPLC conditions as in Figure S3.

References

(S1) Stone, A. *The Theory of Intermolecular Forces*, 2nd ed.; Oxford University Press: Oxford, 2013.

(S2) Tang, K. T. Dynamic Polarizabilities and van der Waals Coefficients. *Phys. Rev.* **1969**, *177*, 108–114.

(S3) Stone, A. J.; Tough, R. J. A. Spherical tensor theory of long-range intermolecular forces. *Chem. Phys. Lett.* **1984**, *110*, 123–129.

(S4) Casimir, H. B. G.; Polder, D. Influence of Retardation on the London–van der Waals Forces. *Nature* **1946**, *158*, 787–788.

(S5) Antoine, R.; Dugourd, P.; Rayane, D.; Benichou, E.; Broyer, M.; Chandezon, F.; Guet, C. Direct measurement of the electric polarizability of isolated C60 molecules. *The Journal of Chemical Physics* **1999**, *110*, 9771–9772.

(S6) Ballard, A.; Bonin, K.; Louderback, J. Absolute measurement of the optical polarizability of C60. *The Journal of Chemical Physics* **2000**, *113*, 5732–5735.